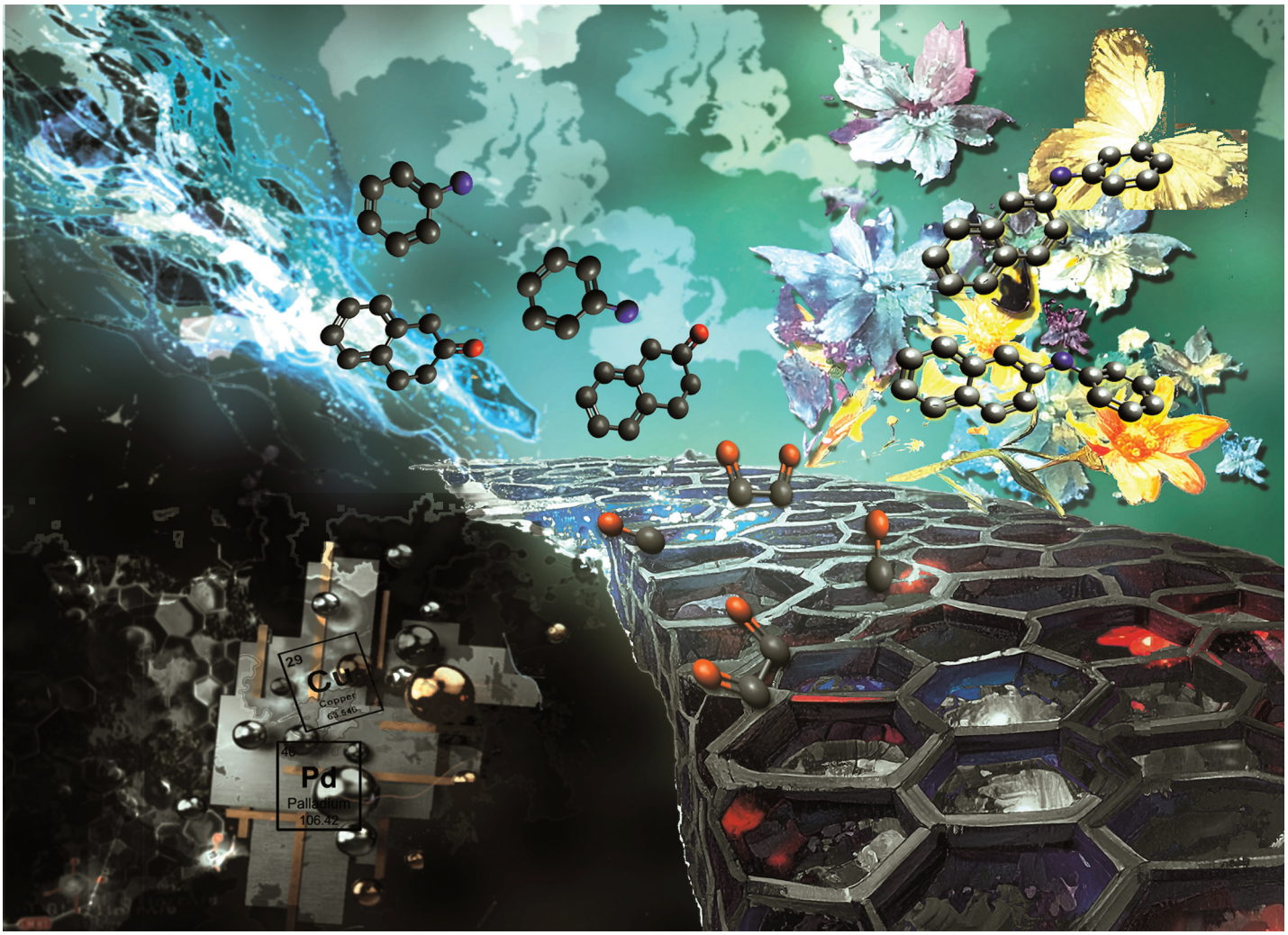

Showcasing research from Dr. Helaja's laboratory, Department of Chemistry, University of Helsinki, Finland. The team focuses on catalytic redox transformations mediated by carbon materials or organophotoredox catalysis.

Cascade synthesis of diarylamines catalyzed by oxygen-rich and porous carbon

Metal-free method to synthesize diarylamines using oxygen-rich, porous activated carbon as the catalyst. The carbon surface simultaneously promotes enamine formation and oxidative aromatization steps, enabling a cascade reaction between anilines and partially unsaturated ketones. The material's porosity plays a key role in stabilizing reactive intermediates and suppressing side reactions, while a molecular *N*-oxide serves as a mild oxidant under inert conditions. The catalyst is robust and recyclable, offering a sustainable alternative to traditional metal-based C–N bond-forming routes.

Image reproduced by permission of Anna Lenarda and Juho Helaja from *Green Chem.*, 2026, **28**, 199.

Cover artwork generated using Adobe Firefly.

As featured in:

See Juho Helaja *et al.*, *Green Chem.*, 2026, **28**, 199.

ROYAL SOCIETY OF CHEMISTRY

rsc.li/greenchem

Registered charity number: 207890

Green Chemistry

PAPER

View Article Online
View Journal | View Issue

Cite this: *Green Chem.*, 2026, **28**, 199

Cascade synthesis of diarylamines catalyzed by oxygen-rich and porous carbon

Anna Lenarda, *[a] Itisha Jain,[a] Aleksi Kaleva,[a] Valtteri Oksanen,[b] Sami Heikkinen,[a] Risto Koivula,[a] Tom Wirtanen,[b] Michele Melchionna,[c] Tao Hu[d] and Juho Helaja *[a]

Received 29th September 2025,
Accepted 29th October 2025

DOI: 10.1039/d5gc05166e

rsc.li/greenchem

Activated carbon derived porous materials, effectively enriched with OH and C=O groups, were found to mediate, in a cascade manner, the condensation between anilines and 3-hexenones or β-tetralones, followed by their aromatization to diarylamines. The reaction proceeds *via in situ* formation of enamine intermediates which are subsequently oxidatively dehydrogenated in presence of a molecular oxidant under inert atmosphere. The functional groups on the carbon surface contributed actively to the catalysis: phenolic hydroxyl groups were found to promote the coupling of amines and ketones to imines and their tautomerization to enamines, while the C=O groups of the quinoidic moieties catalyze the dehydrogenative aromatization step. The carbon material's extensive porous structure turns out to be critical to preserve the reactive β,γ-unsaturated cyclohexanone derivatives and their enamine intermediates from undesirable coupling and condensation side-reactions. The carbocatalyst can be regenerated by molecular *N*-oxo quinoline, which acts as a more convenient and cleaner stoichiometric oxidant in comparison with standard aerobic conditions (oxygen-rich atmosphere). The developed methodology delivered up to 93% yields for many diarylamines, formerly accessible exclusively *via* Pd-mediated couplings. Computational DFT study of possible enamine reaction modes with quinone model compounds, combined with kinetic isotope effects (KIE) suggest that the aromatization reaction is triggered by hydride abstraction at the benzylic position of the enamine intermediate.

Green foundation

1. Our work demonstrates that porous, functionalized activated carbon can replace precious metal catalysts in C–N bond formation, enabling diarylamine synthesis *via* a cascade process under mild conditions. This advances green chemistry by providing a sustainable, metal-free alternative to Pd-mediated couplings with high selectivity and yields.
2. We achieved efficient diarylamine synthesis (up to 93% yield) using a regenerable carbocatalyst and benign stoichiometric oxidant (*N*-oxo quinoline). This eliminates the need for transition metals and halogenated starting materials, while achieving high atom economy through a one-pot cascade reaction.
3. The process could be further improved by employing renewable feedstocks for the carbon material and by regenerating or recycling the stoichiometric oxidant.

1. Introduction

Diarylamines are common substructures in organic molecules relevant to many fields; they are ubiquitous in natural compounds, considered as "privileged structures" in drug discovery and pharmaceutical industry,[1,2] and abundant in both agrochemicals and organic electronics.[3] Contemporary palladium mediated Buchwald–Hartwig[4] and copper mediated Ullmann reaction[5] and Chan–Lam[6] couplings are the most widely utilized synthetic protocols to access them, respectively from amines and arylhalides or arylboronic acids (Fig. 1A). Despite these strategies' advanced state of development, their heavy impact on sustainability and their poor cost effectiveness calls for the development of alternative synthetic routes. The use of saturated, or partially saturated, carbocycles as aryl surrogates, is a known strategy for the construction of aromatic building blocks.[7] In this framework, catalytic oxidative dehydrogenative (ODH) protocols represent an interesting option to access diarylamines. Despite being known in heterogeneous catalysis since the beginning of the twentieth century,[8] the use of ODH in synthetic organic chemistry was

[a]*Department of Chemistry, University of Helsinki, A. I. Virtasen aukio 1, P.O. Box 55, Finland. E-mail: anna.lenarda@helsinki.fi, juho.helaja@helsinki.fi*
[b]*VTT Technical Research Centre of Finland Ltd, P.O. Box 1000, FI-02044 Espoo, Finland*
[c]*Department of Chemical and Pharmaceutical Sciences, INSTM, University of Trieste, Via L. Giorgieri 1, 34127 Trieste, Italy*
[d]*Research Unit of Sustainable Chemistry, Faculty of Technology, University of Oulu, 90014 Oulu, Finland*

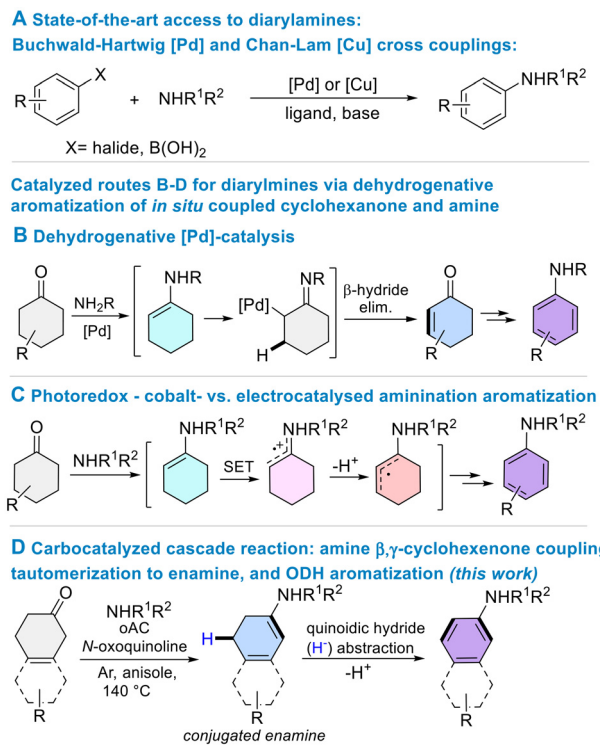

Fig. 1 (A) Contemporary transition metal catalyzed aminations aryl halide *vs.* boric acid; dehydrogenative routes utilizing (B) homogenous and heterogenous [Pd]-catalysis, (C) electrochemical anodic or photoredox-cobalt catalyzed oxidation, (D) carbocatalytic quinoidic ODH associated with their characteristic mechanistic key steps.

proposed only recently by Stahl *et al.*, who reported the formation of phenols from substituted cyclohexanones *via* homogeneous aerobic Pd-catalyzed ODH aromatization.[9] This reaction pathway has been the subject of considerable catalyst development efforts: recently, Yamaguchi *et al.* reported that acceptorless dehydrogenative aromatization of cyclohexanones can be promoted by CeO_2 supported Ni(0) nanoparticles.[10] The concept has been expanded both by Stahl and others by combining it with the well-known reactivity of carbonyl groups with nucleophiles.[11] Several metal free systems have been explored,[12] and in particular, the condensation reaction of cyclohexanones with anilines to form imines, and their subsequent ODH aromatization has been exploited to prepare aryl and diarylamines (Fig. 1B).[13] Aside from palladium, other metals, such as Ir,[14] have been employed as catalyst for the dehydrogenation step, as well as non-metal stoichiometric oxidants, such as elemental sulfur and I_2.[15] Modern avenues to the synthesis of diarylamines involve the use of electro and photocatalysis[16] exploiting single electron transfer (SET) deprotonation routes driven by anodic oxidation or dual photocatalyst cobalt sequences (Fig. 1C). An appealing prospect, demonstrated in several studies, is the use of carbon materials as the catalysts for ODH and acceptorless dehydrogenation reactions.[17,18] Recent research has focused mainly on nanostructured and heteroatom-doped carbons as alternatives to transition-metal catalysts, with their activity attributed to well-defined structural features and proposed active sites.[19] Their practical application, however, is often limited by costly and complex synthesis, low surface area, aggregation, and poor scalability.

In contrast to this trend, we lately proved that air-oxidized commercial activated carbon (oAC) can aromatize partially hydrogenated hetero- and carbocycles. The developed catalytic protocol provides an attractive, alternative to Suzuki–Miyaura couplings, allowing a cost-effective, metal-free access to biaryls[20] and heterobiaryls[21] *via* direct aerobic ODH aromatization. In this study, we employed oAC to promote a cascade route to diarylamines, relying on condensation and ODH aromatization of partially unsaturated cyclic ketones in the presence of anilines (Fig. 1D), where different functionalities on the carbon surface play different roles in the consequent steps of the reaction. In presence of heteroaromatic *N*-oxides as milder molecular oxidants under non-aerobic atmosphere, oxygen sensitive β,γ-arylfused and β,γ-unsaturated cyclohexenones, such as β-tetralone, were successfully converted into a wide range of diarylamines. While the large surface area and extensive porosity characteristic of AC materials, largely exploited for their high adsorption power, have been traditionally considered, for the same reason, cause of deactivation and therefore detrimental in catalysis,[19] we found that these features stabilize herein sensitive substrates and intermediates, suppressing side reactions and enhancing overall efficiency.

2. Results and discussion

2.1 Reaction study and scope

We began our investigation using β-tetralone (**1a**) as the β,γ-unsaturated 3-cyclohexanone derivative, aniline (**2a**) as the aromatic amine partner. oAC_{air}, commercial activated carbon oxidatively treated at 425 °C in air and described in our previous manuscript, was employed as catalyst.[21] Tests carried out in toluene under oxygen atmosphere in presence of 1 equiv. (22.5 mg) of oAC_{air}, conditions typically used for ODH,[21] led to complete decomposition of the starting material in a few hours at relatively low temperatures (50 °C), due to the instability of the ketone under aerobic conditions.

Switching to Ar atmosphere and softer molecular oxidants turned out to be a first turning point. In this regard, our attention was captivated by reports that explored carbon materials' ability to reduce some electron deficient organic compounds, like chlorinated nitroaryls.[22] We first tested 1,4-dichloro-2-nitrobenzene **4** as terminal oxidant. At its best, the catalytic system including 1.5 equiv. of this compound delivered 55% yield of the aromatized product *N*-phenylnaphthalen-2-amine in 24 h at 140 °C under inert atmosphere using anisole as solvent (Fig. 2).

Encouraged by this result, we investigated a series of other known molecular oxidants using the same reaction conditions. Heteroaromatic *N*-oxides have been lately utilized as oxygen source in organic reactions,[23] as oxidants in metal catalysed organic transformations[24] and recognized as oxidants in biological redox reaction.[25] Our screening of variously substituted pyridine *N*-oxides **5–8** with different electronic properties

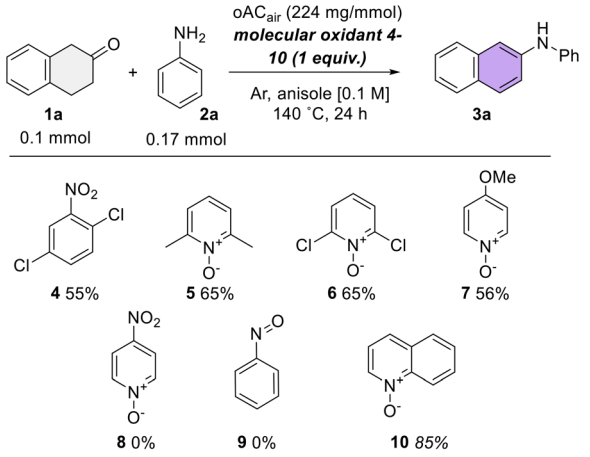

Fig. 2 Screening of various molecular oxidants, reaction conditions: catalyst loading (defined as 1 equiv.) 224 mg mmol^{-1}, 0.1 mmol **1a**, 0.17 mmol **2a**, 0.1 mmol molecular oxidant in 1 mL of anisole.

Table 1 Optimization of reaction conditions[b]

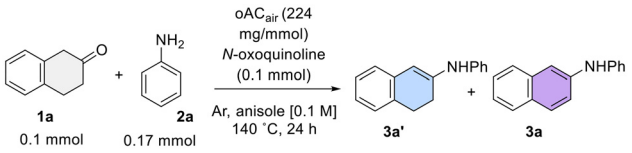

Entry	Variation from optimized conditions	Yield[a] of **3a′**	Yield[a] of **3a**
1	—	0%	85%
2	50 °C in toluene	38%	35%
3	90 °C in toluene	26%	50%
4	110 °C in trifluorotoluene	22%	22%
5	No oAC$_{air}$	6%	15%
6	No oAC$_{air}$, no oxidant (10)	68%	0%
7	0.5 equiv.(112 mg mmol^{-1})[b] oAC$_{air}$	0%	78%
8	2 equiv. (448 mg mmol^{-1})[b] oAC$_{air}$	0%	76%
9	4 equiv. (896 mg mmol^{-1})[b] oAC$_{air}$	0%	78%

[a] Yield is calculated from quantitative ^{1}H NMR (500 MHz, DMSO-d_6) using 1,3,5-trimethoxybenzene as an external reference. [b] Optimized reaction conditions: catalyst loading (defined as 1 equiv.) 224 mg mmol^{-1}, 0.1 mmol **1a**, 0.17 mmol **2a**, 0.1 mmol molecular oxidant in 1 mL of anisole.

delivered the aromatized product in similar fair yields between 55 and 65% except in the case of 4-nitropyridine 1-oxide which, similarly to nitrosobenzene **9**, failed to deliver any observable product (Fig. 2). Lastly, we tested quinoline 1-oxide 10, a widely employed precursor in organic synthesis that has been recently exploited as a nucleophilic oxidant in gold catalysed oxygenative transformations of unsaturated C–C bonds.[26] Employing 1 equiv. of **10**, we were able to obtain *N*-phenylnaphthalen-2-amine **3a** in a satisfying 85% yield.

Any further variation of reaction conditions resulted in lower activities (Table 1). Lowering the temperature to 50 °C and running the reaction in toluene delivered 35% of the fully aromatized *N*-phenylnaphthalen-2-amine product **3a**, together with 38% of the enamine intermediate *N*-phenyl-3,4-dihydronaphthalen-2-amine **3a′** in 24 h reaction time, while increasing the temperature to 90 °C only moderately improved the activity (50%). α,α,α-Trifluorotoluene, another high boiling solvent with higher polarity, delivered only 22% **3a′** and 22% **3a** at 110 °C.

As quinoline *N*-oxide can act as an oxidant on its own,[24] we performed the reaction in absence of oAC$_{air}$ to ensure its catalytic role. The yield obtained in this case was very low (15%), confirming its importance in the developed system. Partially reduced heteroaromatic systems can disproportionate, as reported for 1,2-dihydroquinolines,[27] and the barrier for this reaction has been calculated to be relatively low for *N*-protonated species.[28] To exclude the thermal occurrence of this process from intermediate **3a′** we ran the reaction in absence of both the carbon catalyst and the molecular oxidant: after 24 h at 140 °C, only 68% of **3a′** was observed, with no trace of aromatized product 3a excluding this reaction pathway.

Next, we proceeded to vary the catalyst loading: increasing the loading to 2, and even 4 equivalents, or lowering it to 0.5 equivalents lowered the yield similarly, even if not very significantly, to respectively 76, 78 and 78%, suggesting that 1 equivalent was already the optimal loading. We attribute the lower yield obtained with increased carbon loading to partial, irreversible adsorption of substrates or intermediates on the carbon surface.

The scope of the reaction was then studied, revealing that *para*-substituted anilines, both with electron donating and electron withdrawing groups, are, in general, quite reactive, with small variations in isolated yields (Fig. 3A, entries **2b–2d**). Switching to N-heterocyclic arylamines, however, highlighted a distinct pattern: 2-aminopyridine (**2g**) and pyrimidin-4-amine (**2f**) showed the highest activity, which decreased in the case of *N*-(naphthalen-2-yl)pyridin-3-amine (**3h**), and even more drastically with *N*-(naphthalen-2-yl)pyrimidin-2-amine (**3i**), suggesting a relevant effect of the electronic properties of the arylamine partner.

Methoxy group substitution in different positions on the β-tetralone aromatic ring also affected the reactivity: high yield was obtained with 7-methoxy derivative (**3j**), while 6-methoxy or 5-methoxy β-tetralones turned out to be much less reactive (**3l** and **3m**). The additional methyl substituent in 1-methyl-7-methoxy β-tetralone lowered the yield even further (**3k**). 6-Fluoro substituted β-tetralone produced the highest yield (**3r**). Swapping the aniline with pyrimidin-4-amine (**2f**), which previously showed higher activity did not change the yield obtained with 5-methoxy β-tetralone (**3p**).

To mimic a common substructure in pharmaceutical compounds, **3o**, 7,8-dihydroquinolin-6(5*H*)-one (**1g**) was prepared *via* a reported procedure (see Supporting Information) and successfully reacted with pyrimidin-4-amine. The related diarylamine compound with aniline (**3s**) was also successfully isolated, although in lower yield.

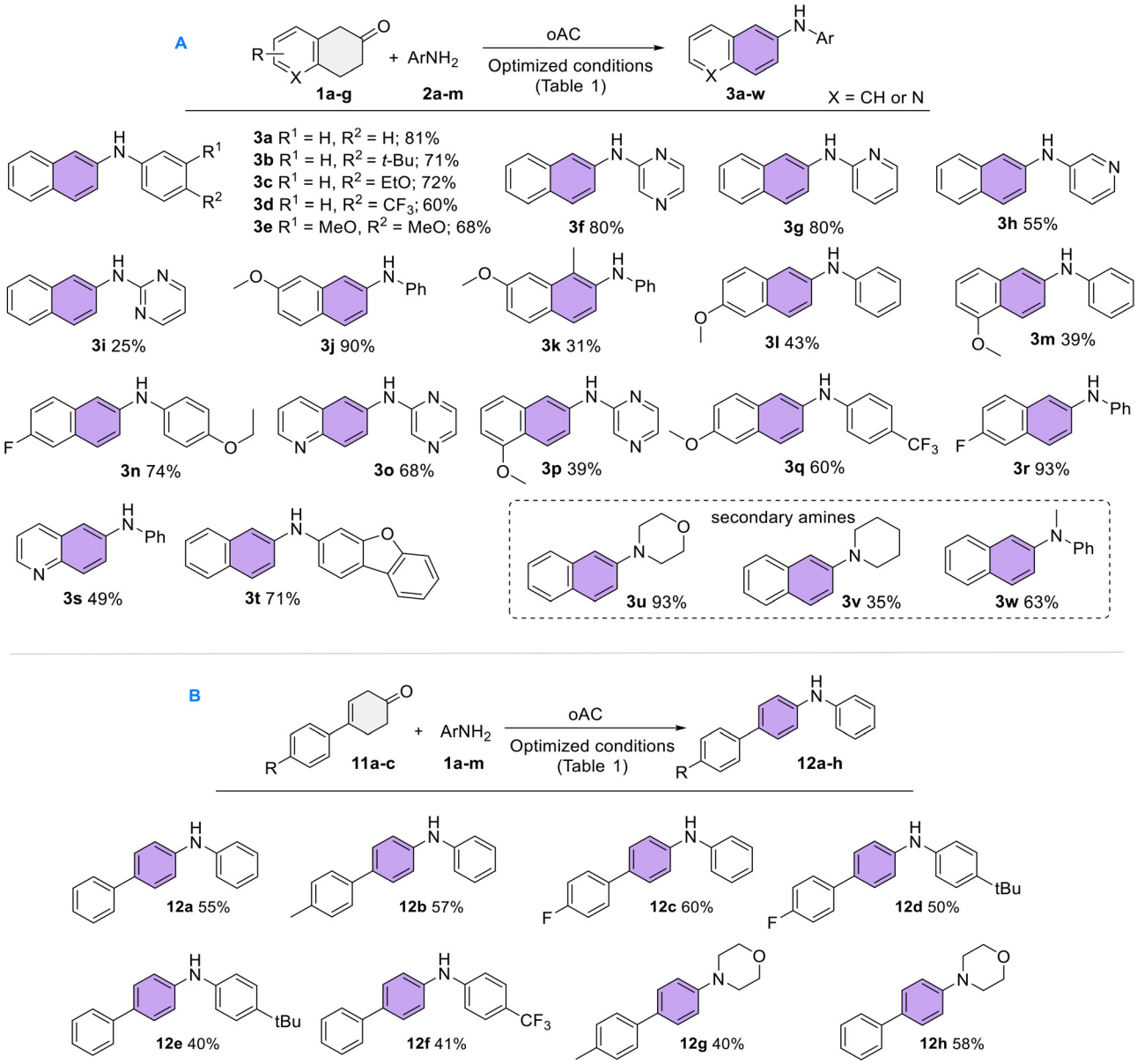

Fig. 3 Scope study of (A) β,γ-arylfused and (B) β,γ-unsaturated cyclohexenones and anilines.

The combination of electron withdrawing and electron donating substituents respectively in the β-tetralone and aniline starting materials resulted in moderate yields (**3n** and **3q**). A larger polycyclic heteroaromatic dibenzo[*b*,*d*]furan-3-amine delivered 71% of aromatized product **3t** when coupled with unsubstituted β-tetralone.

Additionally, two cyclic aliphatic amines, morpholine and piperidine, were tested for widening the scope to a different class of *N*-naphthalene amines. As a result, 4-(naphthalen-2-yl) morpholine **3u** was successfully isolated in high yield, while only 35% of 1-(naphthalen-2-yl)piperidine **3v** was obtained. Finally, employing secondary aromatic amine *N*-methyl aniline delivered 63% yield of product **3w**.

Substituted 4-phenyl cyclohex-3-enones can be straightforwardly synthesized from bromoaryls and 1,4-dioxaspiro[4.5] decan-8-one *via* Grignard reaction followed by subsequent tandem elimination/deprotection (see SI). Interestingly, these compounds could be also used as partially aromatized building blocks to access 4-phenyl anilines, under the optimized conditions. When 4-phenylcyclohex-3-en-1-one **11a** was used as reagent, (Fig. 3B) the product *N*-phenyl-[1,1′-biphenyl]-4-amine **12a** was obtained in 55% yield, and no other product or leftover starting materials was observed in the crude mixture. Lowering the temperature to 110 °C and 90 °C, as well as changing the solvent from anisole to toluene, and all other attempts to optimize the reaction conditions resulted in lower yields (see SI, Table S1).

The scope of the reaction was explored varying the substituent in 4′ position of 4-phenylcyclohex-3-en-1-one and the aniline partner. 4′-Methyl and 4′-fluoro substituted starting

materials delivered similar yield to the unsubstituted one when coupled with aniline (**12b** and **12c**), while both electron rich and electron poor substituents on the amine lowered the yield to 40% (**12e** and **12f**). Any attempt to use electron rich 4′-methoxy substituted aryl substrates produced a complex mixture of products, likely due to an additional coupling step of aromatized ring leading to formation of a mixture non-isolable side product (see SI, Fig. S1). In analogy with the previous scope, cyclic aliphatic amine morpholine was also tested and delivered respectively 40% and 58% yield of biphenyl amine products **12g** and **12h** when coupled respectively with 4′-methyl and unsubstituted 4-phenylcyclohex-3-en-1-one.

2.2 Identification of active sites and catalyst scalability tests

As the surface chemistry of carbon materials is characterized by a complex variety of different functionalities, and several of them have been proposed to be responsible for their catalytic activity, we used a combination of differential experiments and spectroscopic techniques to identify the ones involved in this specific reaction. Our initial hypothesis, based on previous studies by us and others,[17] was that the quinoidic groups on the oAC surface would be the active sites for this catalytic ODH process. To test our assumption, we ran the reaction in the optimized conditions (Table 1, entry 1) with both 4-phenylcyclohex-3-en-1-one **11a** and β-tetralone **1a** using 1 equiv. of phenanthrenequinone (PQ), molecular catalyst which has been used before as a model compound to mimic *o*-quinoidic functionalities on carbon materials.[20,21] From these tests, the desired products **12a** and **3a** were isolated with yields of 40% and 50%, respectively, providing support to our claim. The reactions using 50% loading of the model compound (phenanthrenequinone, PQ) afforded comparable yields of 48% for product **3a** and 35% for product **12a**. The same test performed with anthraquinone as model compound for *p*-quinones, on the other hand, delivered only 20% yield of **3a**. Additional insights on the nature of the active sites were acquired by selectively blocking the C=O, CO_2H and OH groups of oACs (see Materials and methods section 3.1), and running the reaction of **1a** and **2a** in the same conditions with the modified catalysts (Fig. 5a).[29,30] The derivatization of carboxylic acid groups with bromoacetophenone did not cause any major change in yield, suggesting their lack of active participation in the catalytic process. On the contrary, blocking carbonyls with phenyl hydrazine lowered the yield to 50%. The result became even more dramatic when the reaction was run in absence of the molecular oxidant quinoline 1-oxide (10), where only 44% of product could be observed. Interestingly, the esterification of phenolic groups had a considerable effect on the reaction, lowering the product yield to 66%. It seems therefore plausible that phenolic groups are somehow involved in the reaction mechanism, either by being converted to active carbonyls *via* oxidation, or as hydrogen bond donors in their original form.

As additional evidence of the contribution of *o*-quinone moieties to the catalysis, we selectively blocked them by modifying the carbocatalyst with 4,5-difluorobenzene-1,2-diamine, following a procedure reported by Fukushima *et al.*[31] The effective chemical alteration of the desired functional groups was verified *via* XPS analysis (Fig. 4). As summarized in Fig. 4, after the 4,5-difluorobenzene-1,2-diamine labelling, the C=O component decreased from 2.2% to 0.4%, while two new

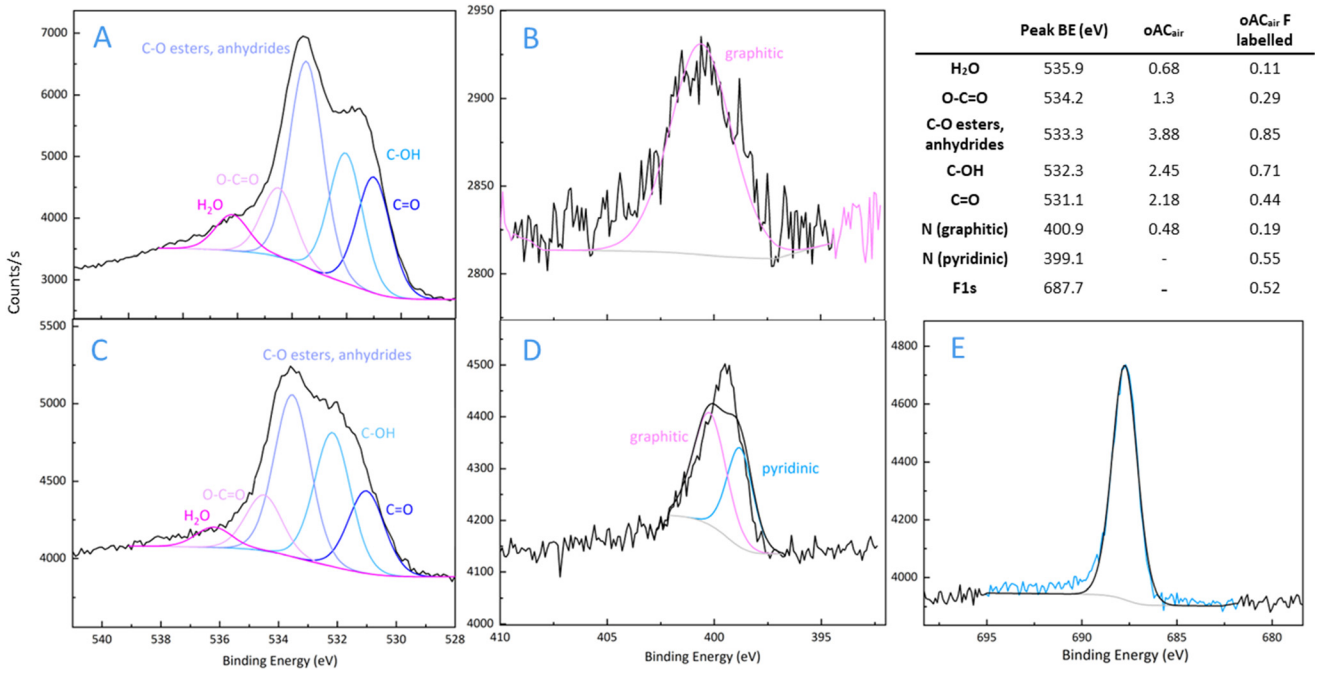

	Peak BE (eV)	oAC_{air}	oAC_{air} F labelled
H_2O	535.9	0.68	0.11
O-C=O	534.2	1.3	0.29
C-O esters, anhydrides	533.3	3.88	0.85
C-OH	532.3	2.45	0.71
C=O	531.1	2.18	0.44
N (graphitic)	400.9	0.48	0.19
N (pyridinic)	399.1	-	0.55
F1s	687.7	-	0.52

Fig. 4 XPS analysis of oAC_{air} before and after 4,5-difluorobenzene-1,2-diamine labelling: summary of O1s deconvolutions (a) and (c), N 1s (b) and (d) and F 1s (e) peaks. Atomic values in Table in %.

signals appear: a lower, pyridinic component in the N 1s region and, more importantly, the characteristic F 1s signal at 687.0 eV.

The reaction run using the F-labelled material as catalyst only delivered 48% of the aromatized product, further confirming the crucial role of *o*-quinone moieties in promoting the reaction. The role of surface chemistry in this catalytic process was explored in more depth using other reference AC materials (see Materials and methods section 3.1.3 for their preparation) characterized by different surface chemistry (Fig. 5b).[21] Both $oAC_{air(\Delta)}$, oAC_{air} treated at 450 °C in inert atmosphere to fully remove carboxylic acid groups, and oAC_{HNO_3}, which oxidation process in concentrated HNO_3 at 140° C makes strongly acidic, did not significantly affect the reaction yield under standard conditions, confirming the low relevance of acidic functionalities for this reaction. Surprisingly, AC_{dm}, simple commercial activated carbon washed with diluted HCl to remove metal impurities with no additional oxidative treatment, exhibited remarkable activity (67%) despite its lower content of surface oxygen groups, even in absence of molecular oxidant quinoline 1-oxide. Similarly, product **3a** was obtained with 77% with oAC_{air} in absence of any oxidant. These findings suggest that carbonyl groups are not the sole factor in determining the catalytic activity, which instead is controlled by a more complicated mechanism than that of other ODH reactions.[21] This idea was in agreement with the relatively low activity observed when we explored reduced graphene oxide (rGO), a widely reported catalyst in ODH,[21] which instead, in this case gave only 50% yield of the main product together with a complex mixture of side products. The relatively high O content in this material, together with its different structural features compared to AC, made us want to investigate the role of porosity and surface area, as it appears to be a critical parameter for the studied reaction. We selected pyrene as an inert polycyclic

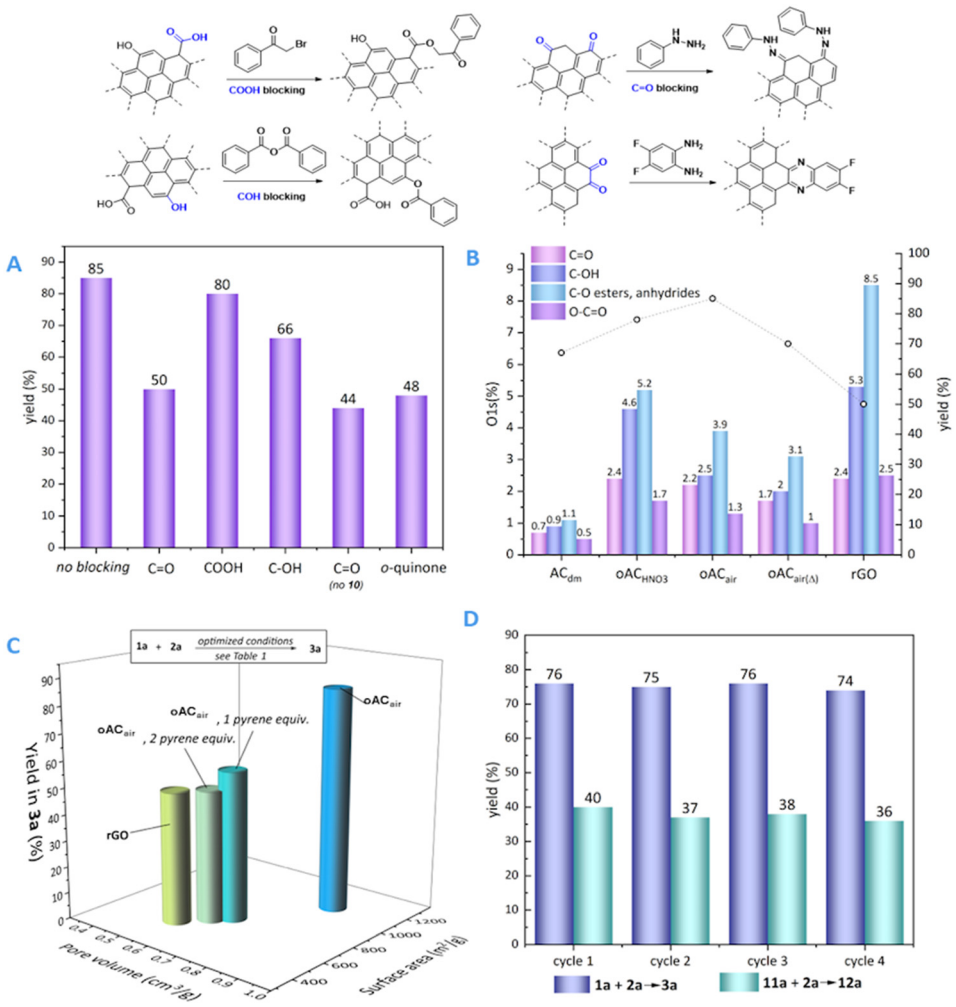

Fig. 5 (A) Catalyst test with oAC_{air} showing effect of selective blocking of functional groups, C═O (without **10**) refers to the experiment run with C═O blocked catalyst in absence of molecular oxidant (B) Atomic percentages from XPS O 1s spectra (bars) and yield in **3a** after 24 h, optimized conditions from Table 1 (dashed line with circles), AC_{dm}, oAC_{HNO_3}, oAC_{air}, and $oAC_{air(\Delta)}$, represent HCl-washed, HNO_3 oxidized, air oxidized, and thermally treated air oxidized active carbons, respectively; rGO represents commercial reduced graphene oxide. (C) Catalyst test with oAC_{air} blocking pores with different pyrene loadings, and (D) Recycling of catalyst over four cycles.

aromatic compound to compete in occupying the pore volume with the substrates and intermediates. First, we ran the reaction in the presence of different amounts of pyrene, to physically block the pores of the appropriate size. We observed that the yield of **3a** dropped to 57% and 50% in the presence of one and two equivalents of pyrene, respectively, as compared to the 85% obtained in absence of the additive. Contrarily, addition of 1 or 2 equivalent of pyrene in the reaction mixture when PQ, molecular model for *o*-quinones, was used as catalyst, did not alter its activity. Incidentally, the yield and product mixture obtained in these conditions is rather similar both to the one obtained with GO, and in the tests with pyrene blocking the pores of oAC_{air}. This seems to imply that the large surface area and extensive porosity, characteristic of AC materials, play a crucial role in promoting the reaction, either by stabilizing the ketone through π–π coordination or favoring its coupling with the aniline partner by increasing their local concentration (Fig. 5b).

To confirm the effect of pyrene in altering the material's pore structure, we stirred oAC_{air} with different amounts of the probe molecule in the same conditions as we perform the catalytic test and, after thorough washing and drying (see Materials and methods, section 3.1), analyzed the samples by means of N_2 physisorption (Fig. 5c). The clear correlation between pyrene loading and decreased surface area confirm its effectiveness in altering the pore structure of the material: the original surface area of over 1000 $m^2\ g^{-1}$ becomes respectively 729 $m^2\ g^{-1}$ and 662 $m^2\ g^{-1}$ in presence of one or two equivalents of blocking probe, in good correlation with the 30% and 40% decrease in yield observed in the related catalytic experiments. A similar trend is evident in the decreased pore volumes (Fig. 5c). The BET analysis of rGO supports this hypothesis: its structural analogy to the pyrene blocked samples (Fig. 5c), results in similar behaviour in catalysis.

Finally, oAC_{air} was analyzed with solid-state ^{13}C NMR (SI, Fig. S8). The spectrum is dominated by the strong band characteristic of graphitic C, which prevents detection of other functional groups.

We then assessed the robustness of the catalyst by carrying out recyclability tests. When oAC_{air} was used, after four sequential 6 h-long catalytic cycles, we did not observe any major decrease in activity, both for the synthesis of *N*-phenylnaphthalen-2-amine and *N*-phenyl-[1,1′-biphenyl]-4-amine (Fig. 5d).

Moreover, scaling up the reaction to 1 mmol scale resulted in no significant decrease of activity (isolated yield 75%). This aspect is encouraging from the point of view of industrial development. Inductively coupled plasma mass spectrometry (ICP-MS) was used to investigate the possible presence of residual metal impurities in the batch of activated carbon employed in this study. The analysis revealed a maximum Fe content of 600 ppm and notably lower levels of other metal impurities. Such trace concentrations are far below the threshold typically associated with catalytic activity, making trace-metal catalysis highly unlikely (reported in a previous publication, see ref. 21). Finally, the headspace of the reaction was analysed *via* MicroGC to evaluate the gaseous products composition. After 16 h reaction time no traces of H_2 were detected, indicating against direct dehydrogenative regeneration of the carbocatalyst (see SI).

2.3 Analysis of reaction mechanism: kinetic measurements

Monitoring of the reaction over time was conducted with ^1H NMR, using oAC_{air} as catalyst. The kinetic study of **1a** with three different amines **2a**, **2g** and **2h**, which form products **3a**, **3g** and **3u**, revealed that the reaction proceeds in a cascade manner *via* conjugation stabilized[32] enamine **3′** intermediates, that are, in a subsequent step, dehydrogenated to the aromatized products (Fig. 6a). Examining the reactions at their early stage shows that the enamine formation is faster for morpholine **2h** than for aniline **2a**, while for 2-aminopyridine **2g** the rate is clearly the slowest. The formation of aromatized product **3u** appears to be the fastest in this monitoring series, but it seems to be a consequence of the high enamine **3u′** concentration in the early stage of the reaction. A closer examination of enamine/product ratios after two-hour reaction time reveals, in fact, that, for **2g**, the yield product is *ca.* 50% of that of enamine, while for **2a** and **2h** the ratio is 40% and 35%, respectively. This implies that, while the enamine limits the rate of product formation, the aromatization proceeds the smoothest for enamine **2g′**.

The rate of formation for the **3′** intermediates can be rationalized by comparing, on the one hand, the different amines' basicity and nucleophilicity, that has been observed to be critical for imine formation rate,[33] and on the other hand, the thermodynamic stabilities of enamines themselves. In fact, both these values increase going from **3g′** to **3a′** to **3u′** (Fig. 6a), in good correlation with what we observed experimentally.

The coupling and tautomerization steps are known to proceed swiftly in protic media under mildly acidic conditions,[34] while without proton shift mediators these steps exhibit high barriers.[35] However, the reaction proceeds smoothly delivering high yields in our optimized catalytic conditions, which make use of relatively dry non-protic solvents such as anisole and toluene.

Herein, we attribute this role to OH and CO_2H functional groups abundantly present on activated carbon surfaces, which can mediate these steps even in the presence of minor amounts of moisture. Kinetic monitoring of the reaction with **1a** and **2a** using three different carbons as catalysts shows that, after 2 h, the enamine formation occurs the fastest with oAC_{air}, which carries an increased amount of these groups compared with AC_{dm}, that can still mediate enamine formation rather well. The reaction, however, proceeds rather modestly with OH blocked oAC_{air} (Fig. 6b), underlining the relevant role of these groups in the formation of **3a′**. To further explore this effect, we studied the reaction kinetics in presence of different, controlled amounts of water (Fig. 6c). Addition of 5 μl of H_2O appears to have a beneficial effect, increasing the rate of the reaction significantly in the first hours. However, the product yield stops improving after 15 h, suggesting the occurrence of competing side reactions in these conditions. The effect is

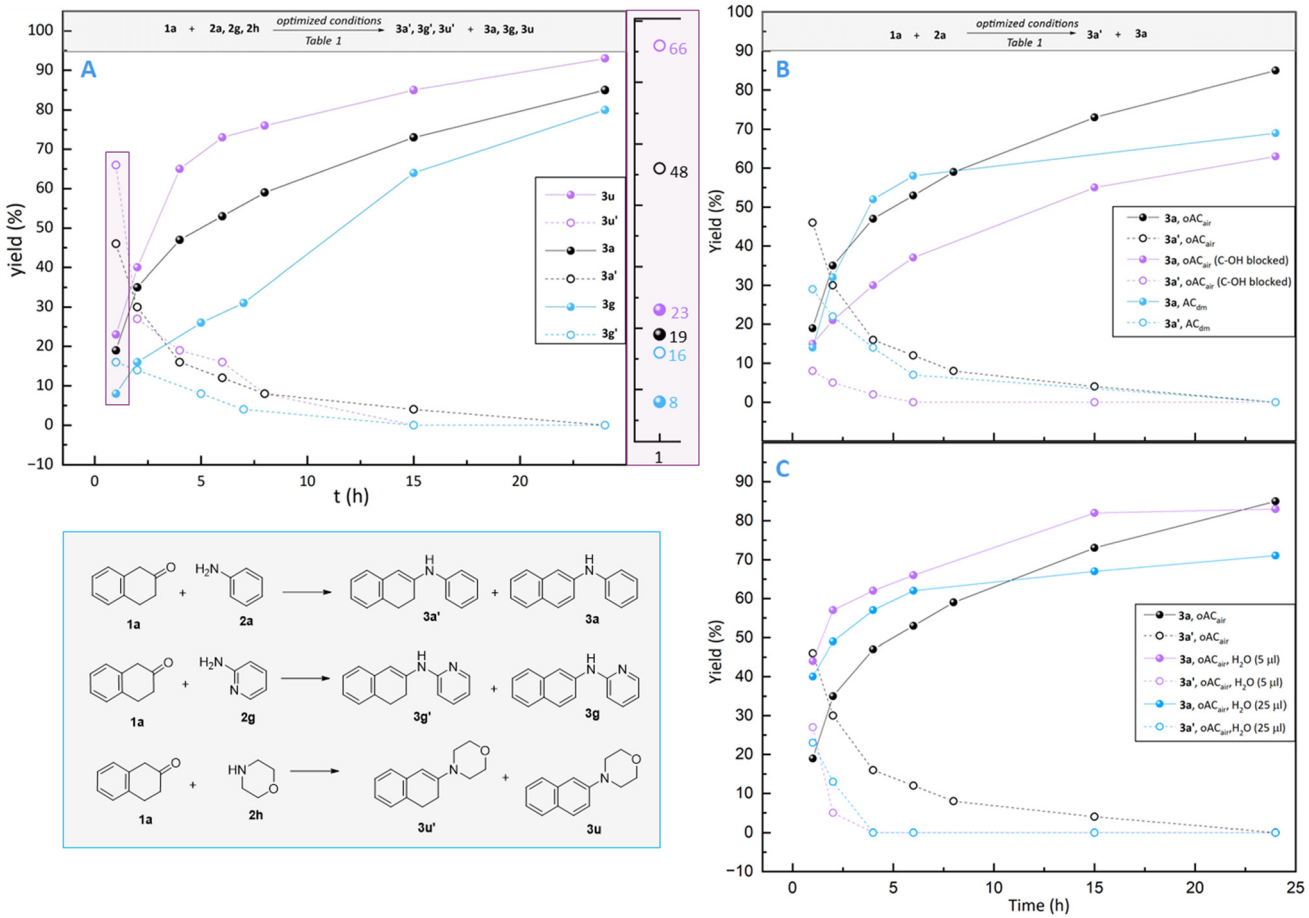

Fig. 6 Kinetic monitoring of catalysis: each point was determined by stopping the reaction and working it up separately; the yield was determined from quantitative ^{1}H NMR (500 MHz, DMSO) of the crude product using 1,3,5-trimethoxybenzene as an external reference (A) **1a** with amines **2a**, **2g** or **2h**, oAC$_{air}$ as catalyst (B) **1a** + **2a** with different carbons as catalyst: plain AC (AC$_{dm}$), air oxidized AC (oAC$_{air}$) and phenolic O-blocked oAC$_{air}$. (C) **1a** + **2a**, oAC$_{air}$ as catalyst, in presence of different amounts of water (5 µl, 25 µl).

even more pronounced when the water addition is increased to 25 µl. Additionally, we carried out kinetic studies with selectively deuterated β-tetralones (Fig. 7). The only KIE (2.9) was received for 4-position deuterated ketone, which indicates that hydrogen/hydride abstraction at the benzylic position forms a reaction barrier affecting significantly the rate of the reaction. This agrees with computed rate-limiting barrier for the aromatization of enamine **3a**′, that is H-4 abstraction by the quinone model (*vide infra*).

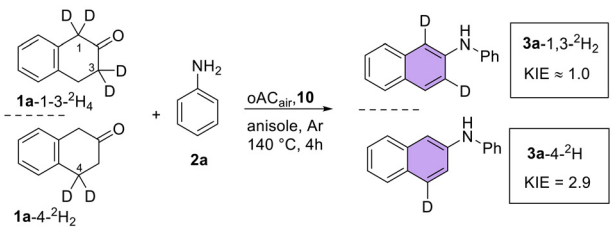

Fig. 7 Kinetic isotopic effect measurements; yield was determined from quantitative ^{1}H NMR (500 MHz, DMSO-d_6) of the crude product using 1,3,5-trimethoxybenzene as an external reference.

2.4 Analysis of reaction mechanism: computational studies

To get theoretical insights and rationalize these observations, we studied the reaction mechanism by means of DFT calculations (M062x/6-31+G(p,d)CPCM(anisole)).

First, we estimated the enamine formation reaction energy for **1a** and amines **2a**, **2g**, **2u** (see SI, Table S5) by applying explicit anisole molecules to dissolve H_2O, obtaining exergonic energies for all conjugated enamines, −5.7, −7.9 and −3.1 (see SI) respectively for **3a**′, **3g**′ and **3u**′, which are in good agreement with what we observed in the kinetic study.

Secondly, we became interested in the imine-amine tautomerization barrier: since the imine tautomer was not observed in the reaction monitoring, despite its formation preceding that of the enamine one, we supposed that a low activation energy for this process, in addition with its favorable thermodynamics, could kinetically explain this behavior. In absence of proton shift mediators, imine–enamine proton transfer scans returned remarkably high barriers (>60 kcal mol^{-1}), sig-

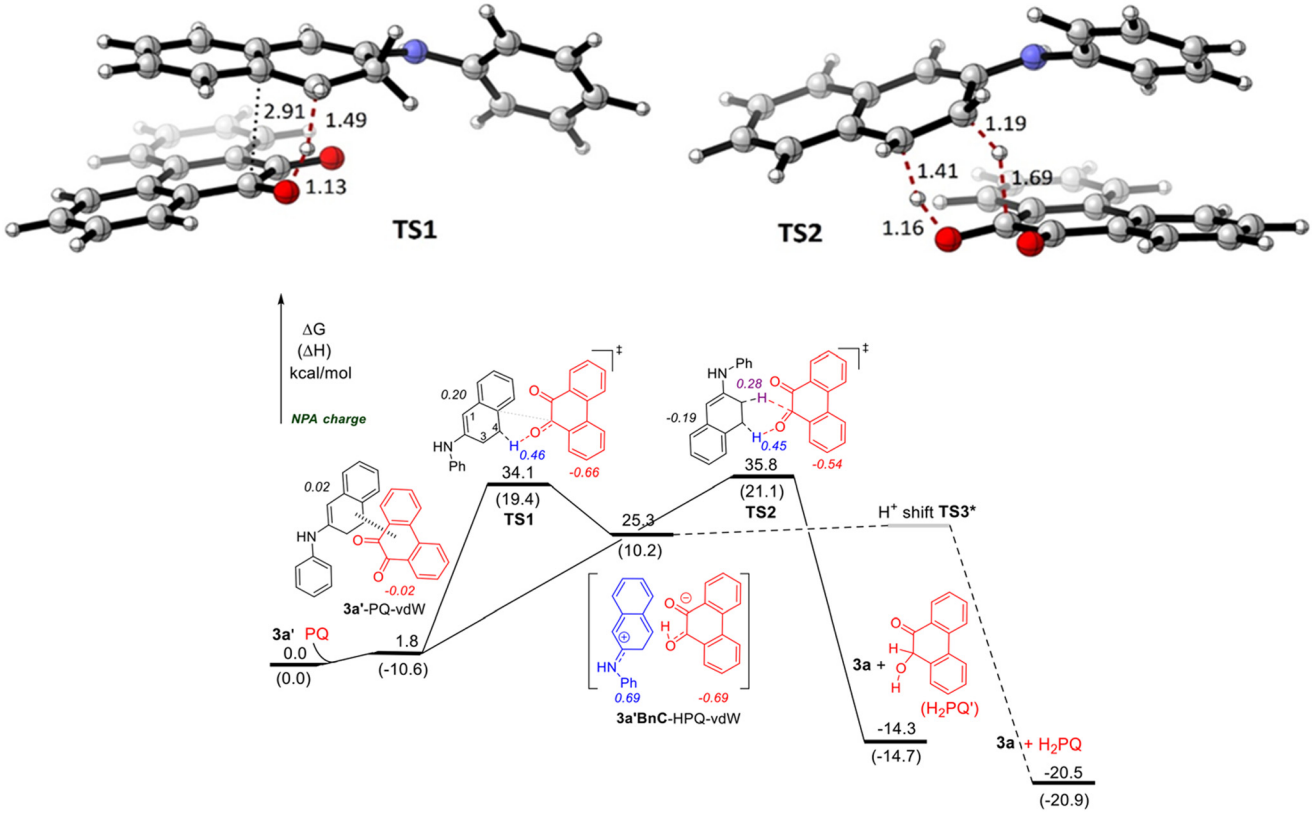

Fig. 8 Enamine **3a′** and PQ hydride shift energy profiles.

nificantly lowered by assisting molecules, as indicated by including two or three H_2O or two H_2O and one phenol (see SI). The calculations performed for imine **3a″** tautomerization to enamine **3a′** report, for example, lower activation energy barriers by assistance of two or three H_2O or two H_2O and one phenol, 28.8, 26.8 and 24.9 kcal mol^{-1}, respectively (see SI, Fig. S9). A similar trend is observed for the exergonic thermodynamic stabilities of all enamines (see SI, Table S6): the barrier for the tautomerization of **3g″** to **3g′**, for instance, if mediated with two H_2O, is 31.3 kcal mol^{-1}.

The activity of PQ as molecular catalyst for this reaction (see section 3.2) justifies its use also as an active site model for the quinoidic functionalities on the carbon surface. Quinones are capable to mediate both open and closed cell redox processes, though typically quinoidic oxidation of organic substrates proceeds *via* polar reaction mechanism involving hydride abstraction.[36] KIE experiments of dihydropyridine compounds with strong hydride/electron donors by Fukuzumi *et al.* have shown that this process operates *via* ion-pair mechanism for electroneutral and mildly electron deficient *p*-benzoquinone derivatives, as demonstrated with chloranil and more electron rich quinones ($E_{0(Q/Q^{\cdot-})}$ < 0.01 V *vs.* SCE), while a radical mechanism is associated to strong electron acceptors, like 2,3-dichloro-5,6-dicyano-1,4-benzoquinone (DDQ) ($E_{0(Q/Q^{\cdot-})}$ = 0.51 V *vs.* SCE).[37] Meanwhile, by studying nicotinamide adenine dinucleotide models as electron/hydride donors and *p*-quinones as oxidants Cheng and coworkers discovered that

Table 2 C–H activation barriers of selected enamines by PQ (and CQ)

Entry	Compound (+H-bond donor)	TS1	TS2
1	**3a′** + H_2O	**30.8**	34.2
2	**3a′** + PhOH	**28.4**	32.2
3	**3g′**	35.6	**33.4**
4	**3u′**	**32.2**	34.9
5	**3j′**	**33.5**	35.2
6	**3l′**	**32.1**	34.4
7	**3m′**	**31.1**	35.2
8	**3a′**/CQ instead of PQ	**31.8**	32.9

The lower of the **TS1**/**TS2** barriers is shown in bold, indicating the preferred stepwise or concerted route, respectively.

empirical 1 V endothermic redox potential limits the radical pathway, while ionic hydride transfer mechanism can operate above this limit.[38]

The measured reduction potential for PQ, obtained *via* cyclic voltammetry, is −0.66 V *vs.* SCE (NBu_4PF_6 0.1 M in MeCN).[39] Computation of oxidation potentials for the studied enamines results in values between 0.25–0.89 V, *vs.* SCE (MeCN) (Table S9, SI) indicating that the 1 V limit is exceeded for all the substrates apart for **3u′**, which had, nonetheless, modest reactivity.

When we applied the computational concept that Floreancig and Liu recently used for benzylic ether C–H bond activation mechanism by DDQ[40] to **3a′** and PQ we could

confirm that single atom transfer (SET) and hydrogen atom transfer (HAT) are the less probable routes (see SI), while the C–H cleavage likely operates *via* hydride shift from the benzylic position of the enamine either in stepwise manner forming a carbocation intermediate (TS1, Fig. 8) or *via* concerted hydride – proton shift (TS2, Fig. 8).

The inspection of the potential energy surface calculated for the hydride shift from **3a′** to PQ (Fig. 8) shows that the initial van der Waals complex **3a′**-PQ-vdW between **3a′** and PQ has an endergonic energy (ΔG = 1.8 kcal mol^{-1}) exhibiting very weak charge transfer character (e**3a′** = 0.02 and ePQ = −0.02). The reactivity from this point proceeds in polar fashion, and as the benzylic (position 4) carbocation of **3a′** Fig. 6 Enamine **3a′** and PQ hydride shift energy profiles for **3a** (kcal mol^{-1}).is *ca.* 9 kcal mol^{-1} more stable than the allylic (position 3), we assume the PQ carbonyl O-attack takes place at this position. For the stepwise hydride shift pathway, in which the H-shift to oxygen is associated with secondary orbital interaction between the carbonyl carbon of PQ and the phenyl ring of **3a′** (see SI) we calculated 34.1 kcal mol^{-1} energy barrier **TS1** and 25.3 kcal mol^{-1} for the endergonic reaction energy of intermediate **3a′BnC**-HPQ-vdW, which, after a low barrier **TS3** proton transfer step delivers the aromatized product **3a** and H_2PQ.

Alternatively, the reaction may proceed in a concerted manner, where the PQ O-attack takes place also at the benzylic position, and another H-shift to its carbonyl carbon is taking place in the same vibrational mode (TS2, Fig. 8). This route has a slightly higher energy barrier, TS2, ($\Delta G^{\ddagger}$ = 35.8 kcal mol^{-1}) and would deliver directly the aromatized product **3a** together with a different acyloin-type isomer of hydroquinone, H2PQ′, which is known from previous studies to be smoothly oxidized back to quinone in presence of O_2.[41] Variation of the amine partner does not have a dramatic effect on this value, except in the case of **3g′** where the concerted pathway is the energetically preferred one (Table 2, entry 3).

Notably, when a water or phenol molecule H-bonds the oxygen of PQ, the reaction becomes less endergonic (Fig. S9, SI), with reaction barriers lowered to 30.8 and 28.4 kcal mol^{-1}, respectively (Table 2), and intermediate charge transfer complexes (**3a′BnC**-HPQ-vdW) becoming more stable

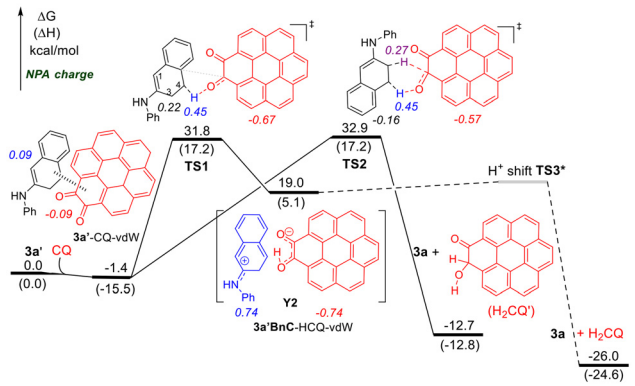

Fig. 9 Energy profile for enamine **3a′** and CQ hydride shift energy profiles for **3a** (kcal mol^{-1}).

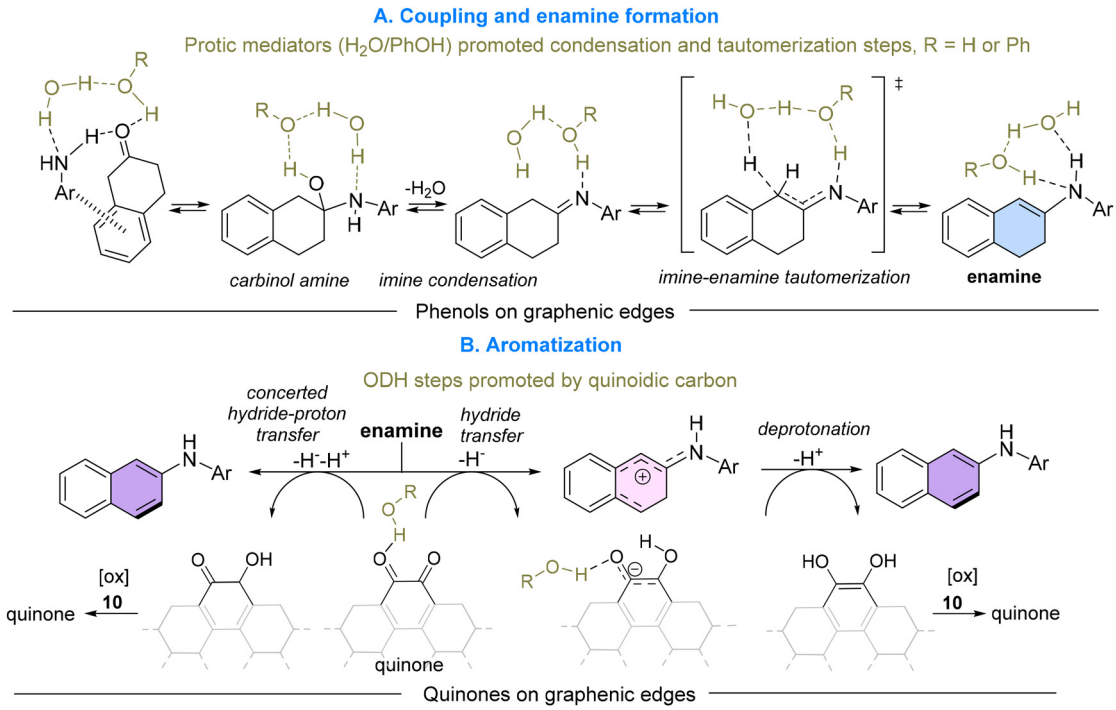

Fig. 10 Mechanistic proposal for the cascade reaction on oAC surface.

although still endergonic (21.2 and 14.4 kcal mol^{-1}, respectively, see SI).

As PQ is a relatively small molecular quinone, we became interested in computing similar C–H activation routes for an o-quinone fused in larger polycyclic aromatic system that is structurally closer to graphene-like carbon materials. Analogous computations performed with coronene-1,2-dione (CQ) as a quinone model compound resulted in a similar energy profile as the one obtained for PQ (Fig. 9). Remarkably, the energy barriers were slightly lower for both the routes, being 31.8 and 31.9 kcal mol^{-1} for **TS1** and **TS2**, respectively; while also the gap between them decreased to 1.1 kcal mol^{-1}. Overall, with CQ as hydride abstractor, the bond forming and breaking distances were similar to those of PQ, however, the charge transfer character of complexes is slightly increased starting from initial vdW-complex (**3a′**-CQ-vdW, e**3a′** = 0.09 and eCQ = −0.09). As the larger coronene platform offers a wider surface for vdW-interactions (NCI plot, SI) and extended conjugation for charge stabilization, the formation energy of the initial vdW-complex becomes exergonic (−1.4 kcal mol^{-1}) and the intermediate complex, **3a′BnC**-HCQ-vdW, 6 kcal mol^{-1} less endergonic (19.0 kcal mol^{-1}). We presume that these factors operate similarly in the studied carbon materials carrying *o*-quinone edges, making both the hydride abstraction routes experimentally possible.

To conclude, we propose that the reaction could proceed on the carbocatalyst surface in a cascade manner (Fig. 10), initiated by coupling of a ketone with an amine, followed by imine condensation and imine–enamine tautomerization steps promoted by protic mediators. The aromatization is then triggered by quinoidic hydride abstraction and completed with deprotonation by hydroquinoidic anion moiety.

While the surface functionalities are key for triggering the catalytic transformation, the material's extensive porosity has the role of preserving sensitive starting material β-tetralone and stabilizing the enamine intermediates.

3. Experimental

3.1 Materials and methods

3.1.1 General remarks. If not described differently, all reactions were performed under air and at RT (18–20 °C). Reactions sensitive to water or oxygen were kept under an inert atmosphere of dry argon, handling them with Schlenk-technique with syringe and septum in absolute and degassed solvents dried on 3 Å molecular sieves prior use. All HPLC-grade solvents were used without further purification as obtained from the supplier (Honeywell, VWR, Merck, Sigma Aldrich). Distilled water was produced with an Aquatron AS4 (Bibby). All commercially available reagents were used without further purification as obtained from the supplier. Column chromatography was executed with pressurized air and at RT over silica gel (pore size 40–63 μm, VWR). All NMR spectra were measured at a sample temperature of 293 K. The following devices were used: Avance Neo 500 (Bruker, 500 MHz), Avance Neo 400 (Bruker, 400 MHz). The chemical shift δ in parts per million (ppm) is relative to the shift of tetramethylsilane (δ = 0 ppm) in both ^{1}H and ^{13}C NMR spectra. The spectra were calibrated to the residual proton or carbon shifts of the corresponding deuterated solvents (^{1}H-NMR: $CDCl_3$ 7.26 ppm, DMSO-d_6: 2.50, ^{13}C-NMR: $CDCl_3$ 77.16 ppm, DMSO-d_6: 39.52). NMR yields were determined with 1,3,5-trimethoxybenzene as an internal standard using a pulse-width of p_w = 3.33 μs and a relaxation delay of d_1 = 35 s. High-resolution mass spectra (HRMS) were obtained using a JEOL MStation JMS-700 (EI) instrument.

3.1.2 General procedure for carbocatalytic reactions. Ketone (0.1 mmol), aniline (15 μl, 0.16 mmol), quinoline-1-oxide (15 mg, 0.1 mmol), anisole (1 mL) and carbocatalyst (22.5 mg, 1 equiv.) were placed in a reaction tube under Ar atmosphere. The reaction mixture was stirred for 24 h at 140 °C. The reaction was cooled to rt, filtered through a pad of Celite and washed with CH_2Cl_2 (50 mL). The solvent was removed under reduced pressure to give the crude product.

3.1.3 Preparation of carbon materials.[21] **AC_{dm}:** 16.0 g of AC (1 kg batch (Lot. H2430) from Fluka with 100 mesh particle size) were placed in a flask and 130 mL of 1 M HCl (aq.) were added. After stirring for 6 h at 70 °C, AC was filtered off and washed with 3 L of dist. H_2O. AC_{dm} was dried in an oven at 140 °C for 16 h and was obtained in a yield of 16.0 g.

oAC_{HNO3}: AC_{dm} (4.00 g) was placed in a flask and 8 mL of nitric acid (68% aq.) was slowly added forming a slurry. The flask was attached to a Dreschel bottle with NaOH aq., and then the flask was heated to 140 °C for 15 h. oAC was then dried in vacuum at 140 °C for 2 h, resulting in a yield of oAC_{HNO3} of 3.88 g.

oAC_{air}: AC_{dm} (4.00 g) was placed in a porcelain crucible which was heated to 425 °C for 16 h (30 °C min^{-1}) in an oven in presence of air. oAC_{air} was obtained in a yield of 3.11 g.

$oAC_{air(\Delta)}$: oAC_{air} (3.11 g) was placed in a tubular oven under Ar flow (40 cm^3 min^{-1}) for 23 h. The temperature was increased from RT to 450 °C (10 °C min^{-1}) and kept at 450 °C for 24 h while maintaining the Ar flow. After cooling to RT, $oAC_{air(\Delta)}$ was obtained in a yield of 3.05 g.

3.1.4 Chemical blocking of functional groups.[29] Carbonyl groups were converted to phenylhydrazones with phenyl hydrazine. Phenyl hydrazine (2.0 g, 18.5 mmol) was dissolved to deoxygenated chloroform (100 mL). oAC_{air} (1.0 g) was added to the solution and mixture was stirred at room temperature for 72 h. To remove unreacted phenyl hydrazine, modified carbocatalyst was Soxhlet extracted for 20 h and washed with chloroform (2 L). Product was dried at 60 °C under vacuum for 24 h.

Phenolic hydroxyl groups were esterified with benzoic anhydride. Benzoic anhydride (5.0 g, 22.1 mmol) was dissolved to deoxygenated chloroform (50 mL), after which oAC_{air} (1.0 g) was added. Mixture was stirred at 60 °C for 24 hours. Modified carbocatalyst was filtered and washed with chloroform (2 L). Product was dried at 60 °C under vacuum for 24 hours.

Carboxylic acids were esterified with 2-bromo-1-phenylethanone. oAC_{air} (1.0 g) and 2-bromo-1-phenylethanone (2.0 g, 10 mmol) were mixed in deoxygenated chloroform (50 mL). Mixture was stirred for 5 h protected from light. Modified car-

bocatalyst was filtered and washed with chloroform (2 L). Product was dried at 60 °C under vacuum for 24 h.

F-labeling of *o*-quinone groups was carried out following a modified reported procedure.[31] 400 mg of oAC_{air} was dispersed in 40 ml of ethanol containing 144 mg (1 mmol) of 4,5-difluorobenzene-1,2-diamine. The reaction vessel was held at 60 °C overnight under an Ar atmosphere. Upon cooling the reaction mixture, the carbon powder was filtered and washed with 500 ml of ethanol and 200 ml of water. The carbon powder was subsequently dispersed in an aqueous 0.1 M $HClO_4$ solution and stirred for 24 h. To avoid possible photoreactions, all reactions were conducted in the dark. Following acid treatment, the carbon powder was filtered and washed with 1000 ml of pure water and dried at 60 °C under vacuum for 24 h.

3.1.5 Physical blocking of pores with pyrene. oAC_{air} (100 g) and pyrene (100 mg or 200 mg, 1 or 2 mass equivalents) were stirred in anisole (5 mL) under Ar atmosphere at 140 °C for 24 h. After cooling down the mixture to rt it was filtered and the carbon residue washed thoroughly with DCM, before drying it in oven at 100 °C for 24 h.

3.1.6 Carbon material XPS measurements. The X-ray Photoelectron Spectroscopy (XPS) analysis was performed by Thermo Fisher Scientific ESCALAB 250Xi XPS System at the Center of Microscopy and Nanotechnology, University of Oulu (Finland). The monochromatic AlKα radiation (1486.7 eV) operated at 20 mA and 15 kV. The powder samples were put in gold sample holder and O, C, N and Au were measured for all samples. The measurement data were analyzed by Avantage V5 program developed by Thermo Fisher Scientific. Charge compensation was used to determine the presented spectra and the binding energies (BE) were calibrated by the C 1s peak position of 284.8 eV. The deconvolution of the peaks was carried out for C 1s and O 1s with Avantage program utilizing peak BE values for groups as reported for carbon materials by Figueiredo and Pereira.[42]

3.1.7 Micro-GC measurements. Reaction was set up following general procedure using 1a and 2a as starting materials and oAC_{air} as catalyst, and run for 16 h in a sealed MW vial. Thereafter, the headspace of was collected into a multi-layer foil sampling bags (SKC Ltd) by purging with N_2 at a rate of 25 mL min^{-1} for 15 minutes. The gas sample was then analysed using an Agilent 490 Micro GC and Agilent OpenLab CDS Chemstation software directly after the sample was collected. Thermal conductivity detector was used in both channels. Channel 1 was fitted with 10 m molecular-sieve column (MS5A) and argon was used as a carrier gas at 100 °C. Channel 2 was fitted PPU column and helium was used as a carrier gas at 80 °C. The apparatus was externally calibrated using known gas mixtures. The samples were fed into the micro-GC at an approximate flow rate of 70 ml min^{-1} using a diaphragm pump and the analysis of the headspace was performed twice. Nitrogen, oxygen and carbon dioxide were detected in the headspace, but no traces of hydrogen were detected. The oxygen and carbon dioxide most likely originate from the transfer lines. The detection limit of H_2 is estimated to 10 ppm.

3.1.8 Carbon material solid-state ^{13}C NMR. The solid-state ^{13}C NMR measurements with DEPTH background suppression[43] (onepuldpth) were performed using an Agilent DD2 600 NMR spectrometer with a magnetic flux density of 14.1 T, equipped with a 3.2 mm T3 MAS NMR probe operating in a double resonance mode. The sample was packed in a ZrO_2 rotor, and the MAS rate in experiments was set to 12.5 kHz. Relaxation delay of 5 s between the scans were used. Protons were decoupled during acquisition using SPINAL-64 proton decoupling. The chemical shifts were externally referenced with adamantane by setting the low field signal to 37.77 ppm.

3.2 Computational details

All geometry optimizations were performed with the range-separated dispersion-corrected M06-2X[44] density functional utilizing a 6-31G+(d,p) basis set, and CPCM solvation model for anisole included in the Gaussian 16 program package.[45] The initial geometries for transition state (TS) search (Berny algorithm – calculated force constants) were found by saddle point crossing distance scans. Intrinsic reaction coordinate (IRC) calculations were done for TS structures (one imaginary frequency) to check their relevance to each reaction step. Single point frequency calculations were performed to obtain Gibbs free energies (DG) with the same functional and solvation model using a larger basis set, 6-311G++(d,p). Biradical TS structure geometries were optimized with the same basis set and solvation model as above using unrestricted UM06-2X functional and guess = mix, always keywords to facilitate symmetry breaking convergence. Cartesian coordinates (*xyz*) of geometry-optimized structures are listed in the end SI together with their free energies and optional imaginary frequencies (for TS's).

4. Conclusions

In summary, we developed an alternative strategy to access diarylamines based on air oxidized activated carbon, operating in catalytic fashion in presence of quinoline *N*-oxide as molecular oxidant. The developed system offers a novel, metal-free route to access a wide scope of substituted *N*-phenylnaphthalen-2-amines in good to excellent yields, including known pharma-relevant substructures, and could be expanded to obtain several *N*-phenyl-[1,1′-biphenyl]-4-amines.

The catalytic behaviour and robustness of the oACs was confirmed by recyclability tests, which showed remarkable stability over four cycles. While carbocatalyst development studies typically focus on determining the active sites and increasing their abundance, here we identified and demonstrated the crucial role of the extended porous structure in the catalyst performance. Their stabilizing effect on both sensitive starting materials and intermediates prevents the occurrence of undesired side reactions, improving its selectivity and the overall efficiency of the process, as was demonstrated by pore blocking experiments with molecular probes.

We anticipate that this work will advance the development of carbon-based catalysts for ODH reactions, providing cost-effective and robust alternatives for transition metal mediated reactions. In particular, the established essential role of their

pore structure for selectivity could be exploited to explore new types of reactivity in these materials.

Author contributions

A. L.: conceptualization, investigation (catalyst development), analysis of results, visualization, writing-original draft; I. J. and A. K.: investigation (synthetic work); V. O.: investigation (H_2 evolution experiments), S. H.: methodology, investigation (NMR), R. K.: resources, investigation (BET analysis), T. W. and M. M.: writing – review & editing; T. H.: resources, investigation (XPS); J. H.: writing – review & editing, resources, project administration, and funding acquisition.

Conflicts of interest

There are no conflicts to declare.

Data availability

All data supporting the findings of this study are available within the article and its supplementary information (SI). Supplementary information: additional catalytic experiments, synthetic procedures, product characterization (NMR including copies of relevant spectra), BET data and spectra, solid state NMR, computational details and XYZ parameters. See DOI: https://doi.org/10.1039/d5gc05166e.

Acknowledgements

We gratefully acknowledge financial support from Academy of Finland (project no. 356338, J.H.) and the Jane and Aatos Erkko Foundation through the Biocat project. Computational resources were provided by CSC , the Finnish National Centre for Scientific Computing.

References

1 (*a*) S. Ekins, K. V. Balakin, N. Savchuk and Y. Ivanenkov, *J. Med. Chem.*, 2006, **49**, 5059–5071; (*b*) O. M. Becker, D. S. Dhanoa, Y. Marantz, D. Chen, S. Shacham, S. Cheruku, A. Heifetz, P. Mohanty, M. Fichman, A. Sharadendu, R. Nudelman, M. Kauffman and S. Noiman, *J. Med. Chem.*, 2006, **49**, 3116–3135; (*c*) J. García-Nafría, R. Nehmé, P. C. Edwards and C. G. Tate, *Nature*, 2018, **558**, 620–623; (*d*) D. A. Horton, G. T. Bourne and M. L. Smythe, *Chem. Rev.*, 2003, **103**, 893–930.

2 D. G. Brown and J. Boström, *J. Med. Chem.*, 2016, **59**, 4443–4458.

3 S. Ke, W. Huang, Z. Zhang, Y. Wang, Y. Zhang, Z. Wu, W. Fang, Z. Wan, Y. Gong, J. Yang, K. Wang and L. Shi, *Front. Chem.*, 2022, **10**, 953523.

4 (*a*) J. F. Hartwig, *Nature*, 2008, **455**, 314–322; (*b*) P. Ruiz-Castillo and S. L. Buchwald, *Chem. Rev.*, 2016, **116**, 12564–12649.

5 (*a*) I. P. Beletskaya and A. V. Cheprakov, *Coord. Chem. Rev.*, 2004, **248**, 2337–2364; (*b*) D. S. Surry and S. L. Buchwald, *Chem. Sci.*, 2010, **1**, 13–31.

6 M. J. West, J. W. B. Fyfe, J. C. Vantourout and A. J. B. Watson, *Chem. Rev.*, 2019, **119**, 12491–12523.

7 S. A. Girard, H. Huang, F. Zhou, G.-J. Deng and C.-J. Li, *Org. Chem. Front.*, 2015, **2**, 279–287.

8 (*a*) A. Skita and H. Ritter, *Ber. Dtsch. Chem. Ges.*, 1911, **44**, 668–676; (*b*) P. Sabatier, *Ber. Dtsch. Chem. Ges.*, 1911, **44**, 1984–2001.

9 Y. Izawa, D. Pun and S. S. Stahl, *Science*, 2011, **333**, 209–213.

10 T. Matsuyama, T. Yatabe, T. Yabe and K. Yamaguchi, *Nat. Commun.*, 2025, **16**, 1118.

11 A. V. Iosub and S. S. Stahl, *ACS Catal.*, 2016, **6**, 8201–8213.

12 K. Deng, H. Huang and G.-J. Deng, *Org. Biomol. Chem.*, 2021, **19**, 6380–6391.

13 (*a*) M. Sutter, M.-C. Duclos, B. Guicheret, Y. Raoul, E. Métay and M. Lemaire, *ACS Sustainable Chem. Eng.*, 2013, **1**, 1463–1473; (*b*) K. Taniguchi, X. Jin, K. Yamaguchi and N. Mizuno, *Catal. Sci. Technol.*, 2016, **6**, 3929–3937; (*c*) L. Wen, L. Tang, Y. Yang, Z. Zha and Z. Wang, *Org. Lett.*, 2016, **18**, 1278–1281; (*d*) S. Takayama, T. Yatabe, Y. Koizumi, X. Jin, K. Nozaki, N. Mizuno and K. Yamaguchi, *Chem. Sci.*, 2020, **11**, 4074–4084; (*e*) Y. Zeng, B. Wang, Y. Li, X. Yan, L. Chen and Y. Wang, *Ind. Eng. Chem. Res.*, 2020, **59**, 1436–1445; (*f*) W.-C. Lin, T. Yatabe and K. Yamaguchi, *Chem. Commun.*, 2021, **57**, 6530–6533; (*g*) S. Pang, Y. Zhang, Y. Huang, H. Yuan and F. Shi, *Catal. Sci. Technol.*, 2017, **7**, 2170–2182; (*h*) H. Li, T. Yatabe, S. Takayama and K. Yamaguchi, *JACS Au*, 2023, **3**, 1376–1384; (*i*) Y. Koizumi, X. Jin, T. Yatabe, R. Miyazaki, J.-Y. Hasegawa, K. Nozaki, N. Mizuno and K. Yamaguchi, *Angew. Chem., Int. Ed.*, 2019, **58**, 10893–10897; (*j*) X. Jin, Y. Koizumi, K. Yamaguchi, K. Nozaki and N. Mizuno, *J. Am. Chem. Soc.*, 2017, **139**, 13821–13829; (*k*) F. Chen, H. Geng, C. Li, J. Wang, B. Guo, L. Tang and Y.-Y. Yang, *J. Org. Chem.*, 2023, **88**, 15589–15596.

14 R. Luo, J. Tong, L. Ouyang, L. Liu and J. Liao, *RSC Adv.*, 2023, **13**, 29607–29612.

15 (*a*) M. Xiong, Z. Gao, X. Liang, P. Cai, H. Zhu and Y. Pan, *Chem. Commun.*, 2018, **54**, 9679–9682; (*b*) Z. Wang, X. Chen, H. Xie, D. Wang, H. Huang and G.-J. Deng, *Org. Lett.*, 2018, **20**, 5470–5473; (*c*) P. Jiang, S. Chen, H. Huang, K. Hu, Y. Xia and G.-J. Deng, *Green Synth. Catal.*, 2021, **2**, 78–81; (*d*) S. Wang, R. Li, S. Jiang, H. Huang, W. Shao and G.-J. Deng, *Adv. Synth. Catal.*, 2022, **364**, 1481–1487; (*e*) H. Wu, L. Zhao, W. Wang, Y. Yu and G. Wu, *Org. Chem. Front.*, 2023, **10**, 5484–5489; (*f*) Z. Wang, C. Li, H. Huang and G.-J. Deng, *J. Org. Chem.*, 2020, **85**, 9415–9423; (*g*) P. Yuan, R. Liu, H.-M. Zhu, Z. Liao, J.-C. Xiang and A.-X. Wu, *Org. Biomol. Chem.*, 2023, **21**, 6468–6473; (*h*) Q. Gao, Y. Guo, P. Cao, G. Fan and Y. Xu, *Chem.*

Commun., 2023, **59**, 13835–13838; (*i*) Y. Shi, C. Yi, X. Huang, Y. Tang, J. Jiao and Y. Li, *J. Org. Chem.*, 2023, **88**, 9554–9564.

16 (*a*) E. Sato, A. Yukiue, K. Mitsudo and S. Suga, *Org. Lett.*, 2023, **25**, 5339–5344; (*b*) S.-K. Tao, S.-Y. Chen, M.-L. Feng, J.-Q. Xu, M.-L. Yuan, H.-Y. Fu, R.-X. Li, H. Chen, X.-L. Zheng and X.-Q. Yu, *Org. Lett.*, 2022, **24**, 1011–1016; (*c*) S. U. Dighe, F. Juliá, A. Luridiana, J. J. Douglas and D. Leonori, *Nature*, 2020, **584**, 75–81.

17 A. Lenarda, T. Wirtanen and J. Helaja, *Synthesis*, 2023, 45–61.

18 (*a*) S. Navalon, A. Dhakshinamoorthy, M. Alvaro and H. Garcia, *Chem. Rev.*, 2014, **114**, 6179–6212; (*b*) C. Su and K. P. Loh, *Acc. Chem. Res.*, 2013, **46**, 2275–2285.

19 (*a*) D. S. Su, G. Wen, S. Wu, F. Peng and R. Schlögl, *Angew. Chem., Int. Ed.*, 2017, **56**, 936–964; (*b*) P. Tang, G. Hu, M. Li and D. Ma, *ACS Catal.*, 2016, **6**, 6948–6958; (*c*) Y. Rangraz and M. M. Heravi, *RSC Adv.*, 2021, **11**, 23725–23778.

20 M. Yang, A. Lenarda, S. Frindy, Y. Sang, V. Oksanen, A. Bolognani, L. Hendrickx, J. Helaja and Y. Li, *Proc. Natl. Acad. Sci. U. S. A.*, 2023, **120**, e2303564120.

21 L. Enders, D. S. Casadio, S. Aikonen, A. Lenarda, T. Wirtanen, T. Hu, S. Hietala, L. S. Ribeiro, M. F. R. Pereira and J. Helaja, *Catal. Sci. Technol.*, 2021, **11**, 5962–5972.

22 J. W. Larsen, M. Freund, K. Y. Kim, M. Sidovar and J. L. Stuart, *Carbon*, 2000, **38**, 655–661.

23 A. Petrosyan, R. Hauptmann and J. Pospech, *Eur. J. Org. Chem.*, 2018, 5237–5252.

24 Y. Wang and L. Zhang, *Synthesis*, 2015, 289–305.

25 R. Teufel, A. Miyanaga, Q. Michaudel, F. Stull, G. Louie, J. P. Noel, P. S. Baran, B. Palfey and B. S. Moore, *Nature*, 2013, **503**, 552–556.

26 Z. Zheng, X. Ma, X. Cheng, K. Zhao, K. Gutman, T. Li and L. Zhang, *Chem. Rev.*, 2021, **121**, 8979–9038.

27 T. P. Forrest, G. A. Dauphinee and S. A. Deraniyagala, *Can. J. Chem.*, 1985, **63**, 412–417.

28 H. Li, J. Jiang, G. Lu, F. Huang and Z.-X. Wang, *Organometallics*, 2011, **30**, 3131–3141.

29 W. Qi, W. Liu, B. Zhang, X. Gu, X. Guo and D. Su, *Angew. Chem., Int. Ed.*, 2013, **52**, 14224–14228.

30 T. Wirtanen, M. K. Mäkelä, J. Sarfraz, P. Ihalainen, S. Hietala, M. Melchionna and J. Helaja, *Adv. Synth. Catal.*, 2015, **357**, 3718–3726.

31 T. Fukushima, W. Drisdell, J. Yano and Y. Surendranath, *J. Am. Chem. Soc.*, 2015, **137**, 10926–10929.

32 (*a*) A. R. E. Carey, G. Fukata, R. A. M. O'Ferrall and M. G. Murphy, *J. Chem. Soc., Perkin Trans. 2*, 1985, 1711–1722; (*b*) E. J. Kikta and J. F. Bieron, *Org. Magn. Reson.*, 1976, **8**, 192–197.

33 C. Godoy-Alcántar, A. K. Yatsimirsky and J.-M. Lehn, *J. Phys. Org. Chem.*, 2005, **18**, 979–985.

34 (*a*) G. M. Santerre, C. J. Hansrote and T. I. Crowell, *J. Am. Chem. Soc.*, 1958, **80**, 1254–1257; (*b*) R. W. Layer, *Chem. Rev.*, 1963, **63**, 489–510.

35 P. J. Silva, *PeerJ Org. Chem.*, 2020, **2**, e4.

36 A. E. Wendlandt and S. S. Stahl, *Angew. Chem., Int. Ed.*, 2015, **54**, 14638–14658.

37 S. Fukuzumi, N. Nishizawa and T. Tanaka, *J. Org. Chem.*, 1984, **49**, 3571–3578.

38 J.-P. Cheng, Y. Lu, X. Zhu and L. Mu, *J. Org. Chem.*, 1998, **63**, 6108–6114.

39 J. Talvitie, I. Alanko, A. Lenarda, N. Durandin, N. Tkachenko, M. Nieger and J. Helaja, *ChemPhotoChem*, 2023, **7**, e202300107.

40 C. A. Morales-Rivera, P. E. Floreancig and P. Liu, *J. Am. Chem. Soc.*, 2017, **139**, 17935–17944.

41 D. Enders and O. Niemeier, *Synlett*, 2004, **12**, 2111–2114.

42 J. L. Figueiredo and M. F. R. Pereira, *Catal. Today*, 2010, **150**, 2–7.

43 D. Cory and W. Ritchey, *J. Magn. Reson.*, 1988, **80**, 128–132.

44 Y. Zhao and D. G. Truhlar, *Theor. Chem. Acc.*, 2008, **120**, 215–241.

45 M. J. Frisch, G. W. Trucks, H. B. Schlegel, G. E. Scuseria, M. A. Robb, J. R. Cheeseman, G. Scalmani, V. Barone, G. A. Petersson, H. Nakatsuji, X. Li, M. Caricato, A. V. Marenich, J. Bloino, B. G. Janesko, R. Gomperts, B. Mennucci, H. P. Hratchian, J. V. Ortiz, A. F. Izmaylov, J. L. Sonnenberg, D. Williams-Young, F. Ding, F. Lipparini, F. Egidi, J. Goings, B. Peng, A. Petrone, T. Henderson, D. Ranasinghe, V. G. Zakrzewski, J. Gao, N. Rega, G. Zheng, W. Liang, M. Hada, M. Ehara, K. Toyota, R. Fukuda, J. Hasegawa, M. Ishida, T. Nakajima, Y. Honda, O. Kitao, H. Nakai, T. Vreven, K. Throssell, J. A. Montgomery Jr, J. E. Peralta, F. Ogliaro, M. J. Bearpark, J. J. Heyd, E. N. Brothers, K. N. Kudin, V. N. Staroverov, T. A. Keith, R. Kobayashi, J. Normand, K. Raghavachari, A. P. Rendell, J. C. Burant, S. S. Iyengar, J. Tomasi, M. Cossi, J. M. Millam, M. Klene, C. Adamo, R. Cammi, J. W. Ochterski, R. L. Martin, K. Morokuma, O. Farkas, J. B. Foresman and D. J. Fox, *Gaussian 16, Revision C.02*, Gaussian, Inc., Wallingford CT, 2019.

